Al-Azhar Bulletin of Science

Manuscript 1681

Section: Physics

Comparison Between Two Global Models Approaches for He + H2O Atmospheric Pressure Radio-frequency Capacitive Discharges

Osama Ahmed Shabaek

Farouk Fahmi Elakshar

Osama Mohamed Yassin

Follow this and additional works at: https://absb.researchcommons.org/journal

 Part of the Biological and Chemical Physics Commons, Computational Chemistry Commons, Computational Engineering Commons, Environmental Chemistry Commons, Fluid Dynamics Commons, Medicinal-Pharmaceutical Chemistry Commons, Numerical Analysis and Scientific Computing Commons, Plasma and Beam Physics Commons, Theory and Algorithms Commons, and the Water Resource Management Commons

ORIGINAL ARTICLE - PHYSICS

Comparison Between Two Global Models Approaches for He + H_2O Atmospheric Pressure Radio-frequency Capacitive Discharges

Osama A. Shabaek*, Farouk F. Elakshar, Osama M. Yassin

Department of Physics, Faculty of Science, Al-Azhar University, Nasr City, Cairo, Egypt

Abstract

In the present paper, we have proposed a chemical kinetic global model to simulate discharge systems with He, working gas, in the existence of different humidity levels. Comparing model results and simulation and experiment in literature establishes satisfaction of model results in qualitative and quantitative levels. The effect of varying model input parameters on densities of OH, H_2O_2, and HO_2 has been investigated. Rising input power increases the yield of the system but raising it over 2W has a minor benefit. Keeping the gas temperature at 300 K has a negligible effect on yield of OH and H_2O_2 and small one on HO_2. Increasing gap distance has decreasing effect on yield, so tradeoff between yield and treated amount of gas would be preferable. We suggest using many devices in parallel to rise treatment rate. Gas flow rate changes the distribution of yield species, so varying it according to desired application is preferable.

Keywords: Atmospheric pressure plasma, Chemical kinetics, Gas discharge simulation, Global model

1. Introduction

Atmospheric pressure discharges have been extensively studied due to various applications particularly environmental and medical applications [1–17]. Because of the difficulties in diagnoses [12,18–39] the need for numerical modelling becomes crucial. Many species and chemical reactions participate in chemically active discharges which motivates researchers to apply various averages over space and time. Averaging over space leads to the development of global models to study atmospheric-pressure chemically active discharges [22,24,40–46]. Alternatively, spatial variation can be considered in fluid or particle models, but it adds high complexity as the computational time becomes very high and the need for very expensive resources becomes crucial which limits exploring the entire parameter space [10].

To investigate the different mechanisms that participate in generating reactive radicals, Liu *et al.* [47], proposed a global model of low-temperature atmospheric-pressure He+H_2O plasmas. Through this work the main species and chemical reactions in He+H_2O plasmas had been identified. According to the simulation results a simplified models capable of capturing the main physicochemical processes in He+H_2O discharges are suggested. In another work, the same group extended their work to contain more reaction species by the addition of Oxygen gas to the discharge model [48]. The effect of water on the chemistry of atmospheric-pressure He+O_2 plasmas was studied by means of a comprehensive global model. Water enables the generation of reactive oxygen species (ROS) mix that are rich not only in O, O_2, and O_2 but also in OH and H_2O_2. In the same direction of research another study has been done by Van Gaens [43] where a chemical gas phase reaction kinetics of noble gas/humid air mixtures with a focus on either components that determine the discharge characteristics or have a biomedical effect. The particle density profiles along the plasma jet had been determined. The effect of varying gas temperature,

Received 2 June 2024; revised 2 July 2024; accepted 20 July 2024.
Available online 24 August 2024

* Corresponding author at. Department of Physics, Faculty of Science, Al-Azhar University, Nasr City, P.O. 11884, Cairo, Egypt.
E-mail address: Oshabaek8@gmail.com (O.A. Shabaek).

https://doi.org/10.21608/2636-3305.1681
2636-3305/© 2024, The Authors. Published by Al-Azhar university, Faculty of science. This is an open access article under the CC BY-NC-ND 4.0 Licence (https://creativecommons.org/licenses/by-nc-nd/4.0/).

flow speed, power density, and air humidity on the chemistry was investigated. Another work had been done by Liu *et al.* [49], in the direction of specifying the main species and reaction pathways that control the main plasma characteristics and chemical species yield of the system. The composition and chemical pathways in Ar+H_2O plasmas have been investigated. A global model that incorporates 57 species and 1228 chemical reactions had been used. Water vapor concentrations from 1 ppm to saturation (32,000 ppm) were considered in the study. Global models give a large amount of data about the reaction species and reaction mechanisms so some researchers prefer to focus on one of important ROS. Naidis [50] in this research concentrates on the production of OH as one of the most important ROS. Results of the modeling of OH production in the plasma bullet mode of cold atmospheric-pressure He−H_2O plasma jets were presented. It was shown that the dominant source of OH molecules is related to the Penning and charge transfer reactions of H_2O molecules with excited and charged Helium particles produced by guided streamers (plasma bullets), in contrast to the case of He−H_2O glow discharges where OH production is mainly due to the dissociation of H_2O molecules by electron impact. In the direction of using plasma with water as a gas trace, Ding *et al.* [40], and his team conducted research to investigate the effect of water gas trace on the plasma characteristics and stability. They used a two-temperature hybrid global model to simulate a chemically complex, bounded, He/H_2O atmospheric pressure discharge, including 43 species with clusters up to $H_{19}O_9^+$. The discharge was embedded in a larger volume, in which the trace gas fraction was controlled, leading to depletion of water within the discharge and diffusive flows of reaction products to the walls. For a planar discharge with a 1 cm electrode radius and a 0.5 mm gap, driven at 13.56 MHz, they determined the depletion and diffusion effects and the α to γ transition, over a range of RF currents (100−1600 A m^{-2}) and external H_2O concentrations (500−10 000 ppm). The transition from the low power α - mode to the high power γ - mode was accompanied by a collapse of the bulk electron temperature, an increase in the density and a decrease in the sheath width. At the highest external H_2O concentration studied, there are no low current (α - mode) solutions because the sheath widths fill the device. The α - mode was recovered at larger gaps (e.g., 1 mm) or higher frequencies (e.g., 27.12 MHz). The higher mass cluster densities decrease rapidly with increasing gas temperature. Alexandra *et al.* [51] compare experiments and global model results of OH densities in a RF atmospheric-pressure plasma in a plane-parallel geometry, operated in Helium with small admixtures of O and H_2O. Simulation results shows that more consistent tailoring of reactive particles mix from the plasma can be achieved by using well-controlled multiple gas admixtures, instead of relying on ambient air mixing. Jing *et al.* [52], applies global model to investigate the role of structured TiO_2 supported by 5% Graphene Oxide in improving NO_x surface association. According to modeling results the researchers can declare the critical role of $NO_{3(ad)}$ in enhancing NO_x production, resulting in efficient $NO_{3(aq)}^-$ generation in water. Zhou *et al.* [53], investigate the regulatory dynamics of three types of reactive Nitrogen species, i.e. NO, N_2O, and ONOOH, by using extended global model comprising 92 species and 1018 reactions. According to simulation results, the authors can clarify the essential intermediate species related to NO, N_2O, and ONOOH generation.

Our proposed global diffusion model, as in basic global models, obtains results in a small computational time if we compare it with fluid or particle models. Small simulation time give us the ability to explore large parameter spaces and to tune all of available parameters to obtain certain desired characteristics for the system. In the present work, we will consider H_2O as an additive to the discharge system, which is considered one of the most important trace gases. The importance of H_2O, in bio-medical and environmental applications, as a gas trace has its potential as the water may arise from contact of plasma with a subject that is being treated. An experiment investigating He+H_2O mixtures has been accomplished [19] and simulated with a global model [47]. The chemistry of water is very complicated, giving rise to many pathways for different species and reactions. In addition, the discharge is weakly electronegative. The researchers [47] compared their extended reaction set, over two ranges of water fraction, to two simplification levels. Their global model, however, used various approximations that lead to significant disturbances from experimental results, as will be seen in section (3).

The structure of the present work is as follows; both simulation models will be presented in detail in section (2). Results and discussion will be presented in section (3) which contains three main parts. Firstly, a comparison between the two models and experimental data will be presented. In the next part an extended comparison between the two model's outputs will be presented. Consequently, the effect of input power, gas temperature, gap distance, and gas flow rate variation will be

investigated. Finally, a conclusion will be given in section (4).

2. Global model formulation

In the present paper two different global models' approaches will be compared with the aim of presenting the most suitable approach for analyzing atmospheric pressure He+H_2O gas discharge. The first approach consists of, a particle conservation equation in addition to a self-consistent solution for the mean electron temperature without solving the energy equation explicitly [47]. The second approach consists of a particle conservation equation in addition to an electron energy conservation equation. The reaction kinetic scheme considered in the present simulations consists of a set of reactions between 46 species through 577 volume reactions (VRs) and 46 surface reactions (SRs). The present group of VRs has been proposed by Liu *et al.* [47].

The proposed system configuration, shown schematically in Fig. 1, has been assumed to consist of two parallel-plate circular electrodes of radius $R = 10^{-2}$ m, and the gap between the two electrodes is 5.0 10^{-4} m. The discharge is assumed to be fed with an RF power source with a frequency of 13.56 MHz and an average power of 11.0 W. The temperature of the gas is assumed to be constant at 300 K, and the gas flow rate is considered to be 0.1 SLM (Standard Liters per Minute). The H_2O impurity level was kept at 1000 ppm (part per million).

In the following part we will present the model proposed by Liu *et al.* [47], and our proposed model in some detail. The species conservation equation gives the change in each particles density with time in the discharge $\partial n_k/\partial t$ and its details and differences between the two models will be presented in the next section.

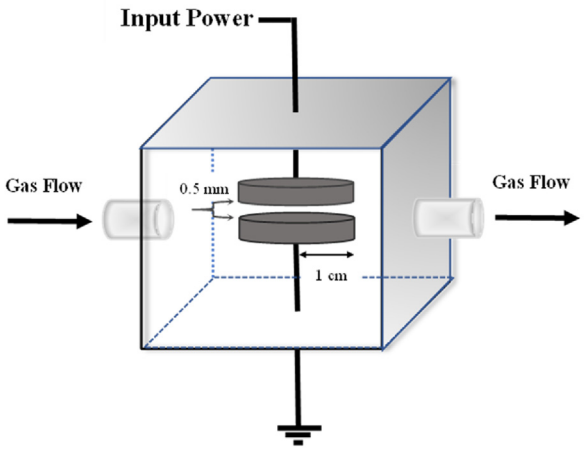

Fig. 1. Schematic diagram for the assumed system.

2.1. Conservation equation for species densities

In the current models the densities of different particles change (generation/consumption) in time, as a result of VRs and SRs. It also takes into account the loss of particles according to, the flux Γ_{2k} through the boundaries out of the plasma region and the flux Γ_{1k} to the electrodesurfaces. In the case of a jet discharge, an additional loss term has to be added according to the flow F_k out of the gap between electrodes.

$$V\frac{\partial n_k}{\partial t} = V\,GV_k + S_1\,(GS_k - \gamma\Gamma_{1k}) - S_2\,\Gamma_{2k} - F_k\,n_k \quad (1)$$

As $n_k(m^{-3})$ is the density of species k, $GV_k(m^{-3}s^{-1})$ the contribution of VRs in the generation/consumption of species k, $GS_k(m^{-2}s^{-1})$ SRs contribution in the generation/loss of species k, $S_1(m^2)$ the area of the electrode where the SRs occur, $S_2(m^2)$ the area of the sides, $V(m^3)$ the volume of discharge, $\Gamma_{1k}(m^{-2}s^{-1})$ the flux of species k to the electrodes surfaces, and $\Gamma_{2k}(m^{-2}s^{-1})$ the flux of particles lost out of the discharge region through the sides. γ is a dimensionless parameter ($0 \le \gamma \le 1$) that represents the probability of reaction occurrence between the incident particles and the surface. $\gamma = 1$ for one species means that all particles of that species react with the electrodes (e.g., positive ions). $\gamma = 0$ for one species implies that no particles of that species lost on the walls at all (e.g., ground-state molecules). In general, however, species can have a specific value of γ, indicating that part of the flux to electrodes bounce back to the plasma and some loses in reaction on the electrode. The particles generated by these surface reactions are added to the particle balance equation in the second term. The last term in equation (1) $F_k(m^3s^{-1})$ is the consumption of chemical species k (only neutrals) due to the flow field.

In the following section, we will present the different terms in the mass conservation equation in more details.

2.2. Volume reactions between species

The change in chemical particles densities depends mainly on the VRs. The considered particles in an interaction has two cases: reactant or product. The particles density of reactants diminishes as it transforms into another species. In the case of a product, the particles density grows as another species transforms into that species.

So, the generation/consumption of particles takes the form:

$$GV_k = \sum_{kp} K_{reac} n_l n_m n_n - \sum_{kr} K_{reac} n_l n_m n_n \quad (2)$$

The first term is the species k generation rate, as a product from the reaction set, where $\sum_{kp}$ is the summation over all chemical reactions where k is one of its chemical products. The second term is the species k loss rate, where $\sum_{kr}$ is the summation over all chemical reactions where k is a reactant. K_{reac} is the reaction rate among the reactants l, m, and n with units of $m^3 s^{-1}$ for two body reactions and $m^6 s^{-1}$ in the situation of three body reactions. n_l , n_m, and n_n are the reactants densities which have units of m^{-3}.

2.3. Surface reactions with electrodes

The surface generation of species k due to the reaction of chemical species i with the boundary surfaces has the form:

$$GS_k = \sum_{i=1, i\neq k}^{N} \alpha_{ik} \Gamma_{1i} \quad (3)$$

Where α_{ik}, the generation probability of chemical species k due to the reaction of chemical species i with the surface and N is the total number of chemical species.

2.4. Fluxes of species to electrodes Γ_1

The considered two models takes two different approaches in representing the species fluxes to electrodes. In the first model by Liu *et al.* [47] the flux Γ_1 for neutrals was estimated according to the thermal velocity v_t.

$$\Gamma_{1k} = \frac{1}{4} n_k v_t \quad (4)$$

Where v_t is the thermal velocity $v_t = \sqrt{8 k_B T_g / \pi m_k}$ as m_k is the mass of species k. On the other hand, in the proposed model the flux Γ_1 for both reactive and nonreactive neutral particles was estimated according to the solution of steady state diffusion equation assuming that $n_i = 0$ at the boundaries, which is satisfied at atmospheric pressure discharges [24]. Accordingly, the flux Γ_1 of both reactive and nonreactive neutrals takes the following expression:

$$\Gamma_{1k} = \frac{12}{V_S} D_k n_k \quad (5)$$

Where V_S is the ratio between volume and electrode area, D_k is the species k diffusion coefficient and n_k is the density of chemical species k. Diffusion coefficients used in the present simulations are given in Table 1.

The present model takes into account the diffusive nature of neutral species which leads to more realistic estimation for neutral fluxes. But diffusive nature of neutrals was not taken into consideration in the model presented in Ref. [4], leading to over estimation in the fluxes to electrodes.

In the model by Liu *et al.* [47] the flux Γ_1 for positive ions was estimated according to the Bohm velocity v_B at the sheath edge. Accordingly, the flux Γ_1 of positive ions takes the following expression:

$$\Gamma_{1k} = n_k v_B \quad (6)$$

As v_B is the Bohm velocity at the sheath edge $v_B = \sqrt{k_B T_e / m_k}$ and T_e is the electron temperature in K. On the other hand in the proposed model the flux Γ_1 for positive ions was estimated by implementing the following formula [24,41,51] for the Bohm velocity at the sheath edge.

$$\Gamma_{1k} = 0.6 \frac{v_B n_k}{\sqrt{(1 + \pi \chi_D / 2\chi_{ion})}} \quad (7)$$

Where χ_D is the Debye length in the sheath and $\lambda\chi_{ion}$ the positive ions mean free path.

The present model considers the effect of positive ions collisions through the plasma sheath which gives more realistic representation for positive ions velocity through the collisional sheath at atmospheric pressure. On the other hand the model presented in Ref. [47] neglects the effect of sheath collisions at atmospheric pressure, it takes positive ion velocity equal to Bohm velocity, leading to

Table 1. Diffusion coefficients of species included in the model.

Species	Diffusion Coefficients (m^2/s)	Reference
He	$8.733 \times 10^{-9}\ Tg^{1.75}$	[18]
H_2O	$4.279 \times 10^{-9}\ Tg^{1.75}$	[18]
He*	$8.733 \times 10^{-9}\ Tg^{1.75}$	[18]
He_2*	$5.923 \times 10^{-9}\ Tg^{1.75}$	[18]
H	$1.558 \times 10^{-8}\ Tg^{1.75}$	[18]
H_2O	$9.2647 \times 10^{-9}\ Tg^{1.75}$	[18]
OH	$4.874 \times 10^{-9}\ Tg^{1.75}$	[18]
OH	$5.508 \times 10^{-9}\ T_g^{1.75}$	[18]
H(n = 2)	$1.558 \times 10^{-8}\ T_g^{1.75}$	[18]
H(n = 3)	$1.558 \times 10^{-8}\ T_g^{1.75}$	[18]
O(^{1}D)	$5.508 \times 10^{-9}\ T_g^{1.75}$	[18]
O(^{1}S)	$5.508 \times 10^{-9}\ T_g^{1.75}$	[18]
O_2	$3.359 \times 10^{-9}\ T_g^{1.75}$	[18]
O_2(b)	$3.359 \times 10^{-9}\ T_g^{1.75}$	[18]
O_2(a)	$3.359 \times 10^{-9}\ T_g^{1.75}$	[18]
OH(A)	$4.874 \times 10^{-9}\ T_g^{1.75}$	[18]
H_2O_2	$3.38514 \times 10^{-9}\ T_g^{1.75}$	[18]
HO_2	$3.61202 \times 10^{-9}\ T_g^{1.75}$	[18]
O_3	$3.21223 \times 10^{-9}\ T_g^{1.75}$	[18]

over-estimation of the positive ions loss due to fluxes to electrodes.

In both models, the flux Γ_1 for negative ions was set to zero, as anions are expected to be prevented from escaping to electrodes because of the ambipolar potential field [40].

Finally, in both models, the electron flux Γ_1 is set to the total flux of positive ions to enforce quasi-neutrality in the discharge.

$$\Gamma_{1e} = \sum_{k}^{N_{pi}} \Gamma_{1k} \tag{8}$$

Where N_{pi} is the total number of positive ions in the system.

2.5. Flux of species through sides Γ_2

In the first model by Liu *et al.* [47], the flux Γ_2 for both reactive and non-reactive neutrals was estimated according to the thermal velocity v_t.

$$\Gamma_{2k} = \frac{1}{4} n_k v_t \tag{9}$$

On the other hand, in the proposed model the flux of neutrals lost out of the discharge region through the sides varies depending on the considered species. Non-reactive species such as H_2, H_2O_2, HO_2 and O_3 are considered to have a flux Γ_2 [24,40,49]:

$$\Gamma_{2k} = \frac{2D_k}{r}\left(\frac{n_{ext}}{n_{H_2O}} + 1\right) n_k \tag{10}$$

Where r is the radius of electrodes, n_{ext}, n_{H_2O} are the external and internal densities of H_2O.

The present model takes into account the radial inhomogeneity of the nonreactive plasma species, due to the diffusion of species out of the system and the diffusion of neutrals into the discharge system, leading to more realistic representation for the fluxes through the system boundaries. On the other hand there is an over estimation in the non-reactive species fluxes in the model presented in Ref. [47] due to the neglection of the radial inhomogeneity.

For reactive species such as O, H and O_2(a) the flux Γ_2 equals [40,49]:

$$\Gamma_{2k} = \frac{\sqrt{12}}{V_S} D_k \frac{n_{ext}}{n_{H_2O}} n_k \tag{11}$$

Where the assumption that $n_k = 0$ at the discharge boundaries, for atmospheric pressure discharges, was taken into consideration at the solution of the diffusion equation.

The present model considers the radial inhomogeneity and high reactivity of reactive plasma species, by the assumption that $n_k = 0$ at the discharge boundaries which is fulfilled according to the high consumption rate at atmospheric pressure, leading to more realistic representation for the fluxes through the system boundaries. On the other hand there is an over estimation in the reactive species fluxes in the model presented in Ref. [47] due to the neglection of these effects.

In both models the flux Γ_2 for charged particles is set to zero according to the consideration that the drift of charged particles is generally in the field direction toward powered electrode.

2.6. Considered volume reactions

In the present paper, the same reaction set that was proposed by Liu *et al.* [47] has been considered in both models. The considered species are He, He*, He^+, He_2*, He_2^+, HeH^+, H, H (n = 2), H (n = 3), H^+, $H_2O_2^-$, $H_2O_3^+$, H_3O^+, $H_3O_2^-$, $H_4O_2^+$, $H_5O_2^+$, O_2^+, O_2^-, O_3, OH, OH (A), OH^+, OH^-, HO_2, H_2O, H_2O^+, H_2O_2, H^-, H_2, H_2^+, H_3^+, O, O (^{1}D), O (^{1}S), O^+, O^-, O_2, O_2 (a), O_2 (b), $H_5O_3^-$, $H_7O_3^+$, $H_9O_4^+$, $H_{11}O_5^+$, $H_{13}O_6^+$, $H_{15}O_7^+$ and electrons.

2.7. Considered surface reactions

In the present paper, SRs are considered for all species. The same surface reaction probability was considered for both models. Excited neutral particles are assumed to go to ground state when they reach the surfaces. Positive ions are assumed to be neutralized as they reach the electrodes [25,54], and no secondary electron emissions have been considered in both models. All negative ion reaction probabilities with the walls are considered to be zero. All electrons that reaches electrodes will be lost. The complete set of wall reactions is presented in Table 2.

2.8. Electron energy calculation

In the model proposed by Liu *et al.* [47] the mean electron energy was estimated self-consistently without solving the energy equation explicitly by implementing the following algorithm. First, they fix the initial electron density to be the desired value, e.g. $n_e = 0.01$ ppm. Then, in each iteration the electron energy is chosen such that the electron density balance has no changes. Therefore, the electron number remains at its starting value. Once the electron mean temperature has been obtained, the particle balance for the rest of the species will be

Table 2. Wall reactions included in the model.

Surface Reaction	Probability	Reference
M^{+a}+Wall → X	1	[40]
He*+Wall → He	1	[47]
He_2*+Wall → 2He	1	[47]
H+Wall → 0.5H_2	3.00E-02	[54]
O+Wall → 0.5 O_2	2.00E-02	[55]
H(n = 2)+Wall → H	1	[47]
H(n = 3)+Wall → H	1	[47]
O(^{1} D)+Wall → H	1	[55]
O(^{1} S)+Wall → H	1	[55]
O_2(b)+Wall → O_2	2.00E−02	[55]
O_2(a)+Wall → O_2	4.00E−04	[25]
OH(A)+Wall → OH	1	[47]
H_2O_3++Wall → H_2O+O_2	1	[40]
$H_{2n+1}O_n^{+b}$+Wall → nH_2O+H	1	[40]
H_4O_2++Wall → 2H_2O	1	[40]
He_2^++Wall → 2He	1	[40]
HeH^++Wall → He+H	1	[40]
H_3^++Wall → 1.5H_2	1	[40]

[a] M stands for He, H_2, H_2O, OH, H, O, O_2.
[b] n = 1,2 … 7.

solved. The process will be repeated until steady state reached. For more details the reader can take a look on reference [47].

In our proposed model the electron temperature has been estimated by solving the power balance equation where the mean electron energy changes in time according to the balance between the rate of energy fed to the system, the electron energy loss due to VRs E_l and the energy consumption because of escaping of electrons and positive ions from the discharge across the sheath.

$$\frac{V}{S_1}\frac{d}{dt}\left(\frac{3}{2}n_eT_e\right)=\zeta\frac{P_{in}}{eS_1}-\frac{V}{S_1}E_l-\epsilon_e\Gamma_{1e}-\sum_{k=1}^{N_p}\epsilon_p\,\Gamma_{1k} \tag{12}$$

Where n_e is the density of electrons, T_e the mean electron temperature, ζ the part of power coupled to electrons, ϵ_e and ϵ_p are the energy lost per electron and ion that escape from the plasma through the sheaths.

The total electron energy loss due to VRs E_l takes the form:

$$E_l=\sum_{j=1}^{N_{eir}}\epsilon_jK_{reac}n_ln_mn_n \tag{13}$$

Where the summation will be performed over all N_{eir} electron impact volume reactions. With a reaction rate K_{reac} and n_l, n_m and n_n are first, second and third reactant densities. The electron energy consumed in a single reaction j equals ϵ_j. P_{in} has been set to constant value of 11 W, which is considered to be acceptable for a RF atmospheric pressure discharge [42]. In electronegative plasmas an appreciable amount of current is carried by positive ions, accordingly the input power will be separated among electrons and positive ions. So the amount of power coupled to electrons can be assumed as [42]:

$$\zeta=\frac{\mu_en_e}{\mu_en_e+\sum_i\mu_in_i} \tag{14}$$

Where μ_e and μ_i are the mobilities of electrons and positive ion species i respectively. Species mobilities used in the present simulations are given in Table 3.

The energy lost for each electron reaching the walls was considered to be $2T_e$ [24] and for the case of positive ions ~ 50 eV [47].

3. Results and discussion

In the current section we will present the results of both models, a comparison between the two models results and experimental data and the proposed model simulation outcomes for the effect of varying different input parameters on some important species densities.

To choose the most suitable model for representing the chemical kinetics in the proposed discharge system a comparison between the two models and experimentally Ref. [34] measured densities of OH species will be applied.

3.1. Comparison between experimental/simulation of OH densities

In the present section we will compare between model in Ref. [47] simulation results, the proposed

Table 3. Mobility of species included in the model.

Species	Species Mobility (m^2/V.s)	Reference
He^+	3.624 × 10^{-6} T_g	[18]
H_2^+	1.106 × 10^{-5} T_g	[18]
H_2O^+	9.014 × 10^{-6} T_g	[18]
OH^+	9.062 × 10^{-6} T_g	[18]
H^+	1.076 × 10^{-5} T_g	[18]
O^+	9.116 × 10^{-6} T_g	[18]
O_2^+	7.907 × 10^{-6} T_g	[18]
$H_2O_3^+$	7.748 × 10^{-6} T_g	[18]
H_3O^+	8.97 × 10^{-6} T_g	[18]
$H_4O_2^+$	7.858 × 10^{-6} T_g	[18]
$H_5O_2^+$	7.858 × 10^{-6} T_g	[18]
$H_7O_3^+$	7.722 × 10^{-6} T_g	[18]
$H_9O_4^+$	7.657 × 10^{-6} T_g	[18]
$H_{11}O_5^+$	7.617 × 10^{-6} T_g	[18]
$H_{13}O_6^+$	7.591 × 10^{-6} T_g	[18]
$H_{15}O_7^+$	7.572 × 10^{-6} T_g	[18]
He_2^+	6.48 × 10^{-6} T_g	[18]
HeH^+	3.438 × 10^{-6} T_g	[18]
H_3^+	1.106 × 10^{-5} T_g	[18]

model in the present paper, and the experimental data published in Ref. [34] at nearly the same conditions applied in the experiment. Both simulations were performed at 1 W input power, 1.4 SLM flow rate, 1 mm distance between electrodes, and gas temperature of 350 K at atmospheric pressure.

Figure 2 represents the effect of different humidity percentages on the yield of OH species. It can be seen that experimentally the density of OH increases sharply as the humidity level increases from 0 to nearly 1000 ppm then it reaches saturation at nearly 4000 ppm of H_2O. Generally, both simulation models show the same qualitative behavior. On the other hand, the quantitative agreement between the proposed simulation model results and the experimentally measured data is very satisfying, validating the certainty of assumptions proposed in the present model. On the other hand the results of Ref. [47] simulation model are two orders of magnitudes smaller than the experimental data, reflecting the greater consumption of species, than in the experiment, due to over estimation in the species fluxes assumed in that model.

Accordingly, both models can be used in investigating the chemical kinetic behavior of a discharge system in a qualitative manner but only the proposed model results can be considered for quantitative results.

In the next section, we will compare between the simulation results of both models for all proposed chemical species.

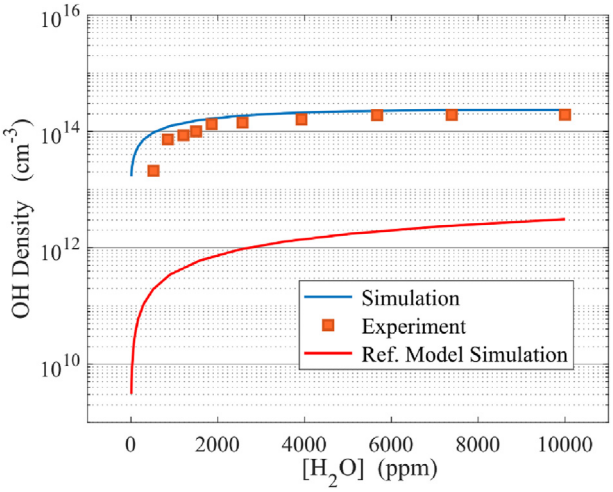

Fig. 2. Comparison between the OH density, as a function of water concentration in the gas mixture, according to the proposed model in the present paper (blue solid line), the experimental data published in Ref. [34] (orange square dots) and simulation results for the model in Ref. [47] (rid solid line), at nearly the same conditions which applied in the experiment.

3.2. Comparison between both models outputs

In the present section we will represent the results for both models at simulation conditions of 1000 ppm H_2O additions, 11 W input power, 0.1 SLM flow rate, 0.5 mm distance between electrodes and gas temperature of 300 K at atmospheric pressure.

Figures 3–7 shows bar graphs with two bars for each selected species density, the first one (in blue) represent the proposed model simulation results, and the second one (in orange) represents the results of the simulation model in Ref. [47].

Simulation results of the proposed model for long-lived species is more than one order of magnitude greater than that of Ref. [47] as can be seen in Fig. 3. The greater long lived species densities in the present model results reflects the lower consumption due to fluxes to the boundaries.

For short-lived species, in general, the densities obtained from the proposed model are greater than that obtained from the model in Ref. [47] except for the case of He* and OH (A) as shown in Fig. 4. In general, the greater short-lived species densities in the present model results reflects the lower consumption due to fluxes to the boundaries, with respect to that in Ref. [47], as in the case of long-lived species. The slight decrease in He* and OH (A) can be explained according to the increase in the consumption rate of those reactive species due to the increase in the densities of partner reactants in loss volume reactions.

In the case of negative ions, generally the densities obtained from the proposed model are less than that obtained from the model in Ref. [47] except for the case of O_2^- as can be seen in Fig. 5. The difference

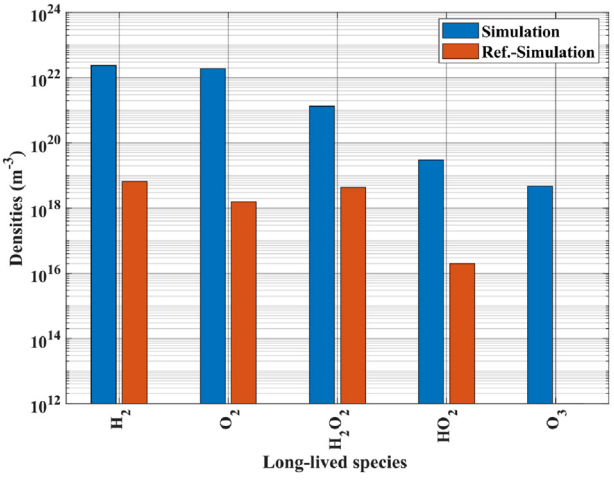

Fig. 3. Comparison between long-lived neutral species densities obtained by using simulation model in Ref. [47] and the one we get by using the model proposed in the present paper.

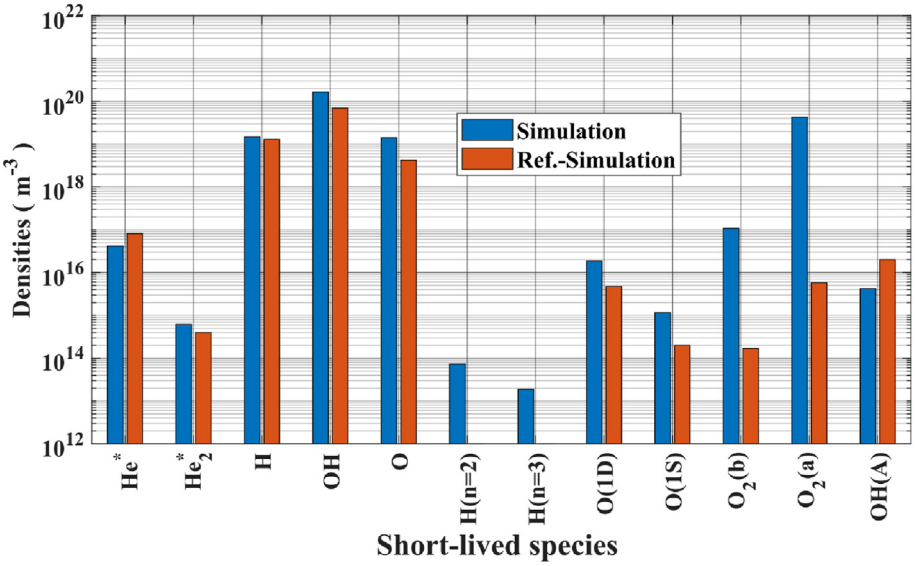

Fig. 4. Comparison between short-lived neutral species densities obtained by using simulation model in Ref. [47] and the one we get by using the model proposed in the present paper.

between the negative ion densities in both models' results can be explained according to the change in the chemical pathways through volume reactions due to the change in the distribution of species in both situations.

For positive ions, generally, the densities obtained from the proposed model are greater than that obtained from the model in Ref. [47] except for the case of H_2O^+ and OH^+ as seen in Fig. 6. The difference between the two model's results can be explained according to the term that represents the positive ions fluxes out of the system, which is in the present model nearly two orders of magnitude lower than that in reference. The slight decrease in H_2O^+ and OH^+ can be explained according to the increase in the consumption rate of those reactive species due to the increase in the densities of partner reactants in loss volume reactions.

As special case of positive ions, positive ion water clusters densities obtained from the proposed model generally are greater than that obtained from the model in Ref. [47] except for the case of $H_5O_2^+$ as shown in Fig. 7. The difference between the two model's results for positive ion water clusters densities has nearly the same characteristics as the case of positive ions.

For more assurance about the proposed model results' relevance and applicability of the study's

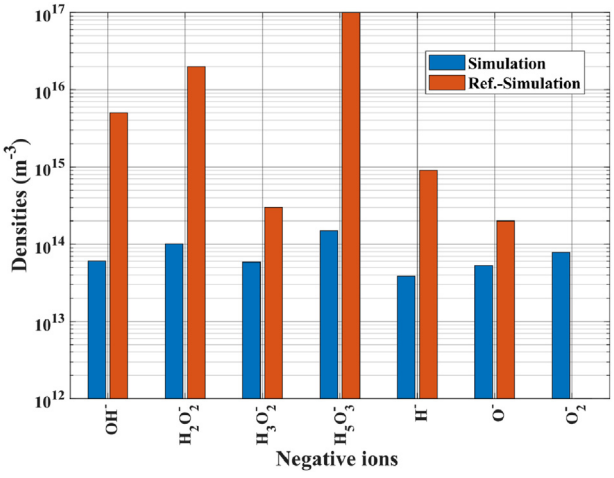

Fig. 5. Comparison between negative ions densities obtained by using simulation model in Ref. [47] and the one we get by using the model proposed in the present paper.

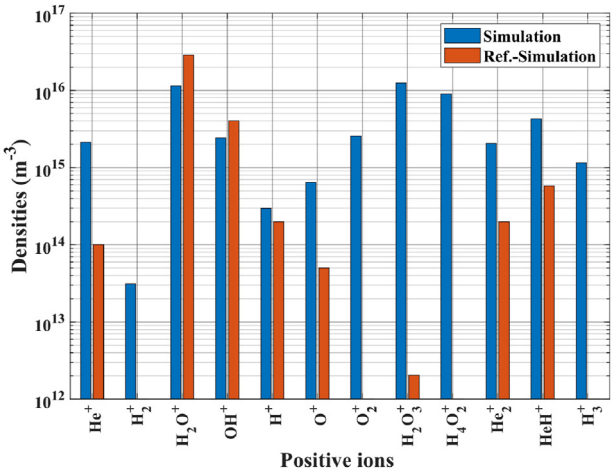

Fig. 6. Comparison between positive ions densities obtained by using simulation model in Ref. [47] and the one we get by using the model proposed in the present paper.

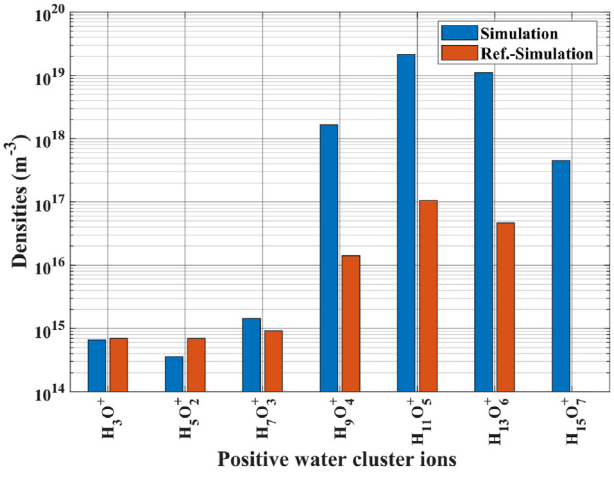

Fig. 7. Comparison between positive ions water cluster densities obtained by using simulation model in Ref. [47] and the one we get by using the model proposed in the present paper.

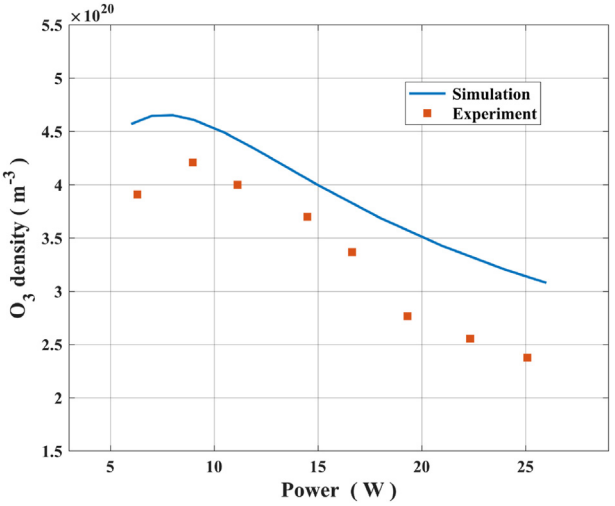

Fig. 8. Comparison between simulation results and experimental measurement [56] for the density of O_3 at different applied input power.

findings to real-world scenarios, We will represent a comparison between the model's simulation results and experimental data in Ref. [56], for the effect of varying the input power to the system on the density of O_3 species, in the next section.

3.3. Simulation versus experiment for different input powers

In the present section we will apply a comparison between model's results and experimental data in Ref. [56], for the effect of different input power on the density of O_3 species. The experiment by Wijaikhum [56] was applied on an rf atmospheric-pressure plasma source based on the COST microplasma jet with He + 0.5% O_2 as a working gas at 10 slm flow rate and 1 mm gap distance. The simulation was applied on nearly the same input conditions as that in the experiment.

It can be seen from Fig. 8 that the simulation model represents the experimental data in both a qualitative and quantitative manner, in the limits of experimental and simulation uncertainties. The O_3 density increases with the input power to maximum value then it decreases gradually with further increase in the input power. Experimental uncertainties include uncertainties in measuring the effective input power and systematic error in O_3 density measurement techniques. Uncertainties in simulation results mostly come from the used reaction rate coefficients [36,37] and the approximations taken in the model. According to the former comparison the applicability of the proposed model for different input parameter has been demonstrated on both qualitative and quantitative levels.

Global simulation models, with very efficient computations and small simulation time, facilitate the investigation of a large portion of the entire parameter space. The ability to investigate many simulation conditions simplifies the process of selecting the appropriate discharge conditions for each gas discharge applications. In the next sections, we will investigate the effect of different input parameters (power, gas temperature, gap distance, and gas flow rate) in tailoring the yield of some important product species (OH, H_2O_2, and HO_2) of the discharge system.

3.4. Important species density variation with input power

The energy consumption is one of the most important aspects in the process of validating any modern treatment method. So, the effect of input power variation on the plasma reactivity has to be investigated as an important indicator in validating the treatment efficiency with respect to input power. In the present section we will represent the results that describes the effect of input power on the density of OH, H_2O_2, and HO_2 as important species in the field of water treatment. Input power to the model was varied in the range from 0.5 to 6.5 W.

Figure 9 shows bar graph that represents the relation between the density of important species in units of cm^{-3} and the input power in W. It can be seen from Fig. 9 that the density of OH radical increases sharply as the input power changes from 0.5 to 2 W but as the input power increases the OH density increases slightly. The densities of both H_2O_2 and HO_2 show the same behavior as the OH

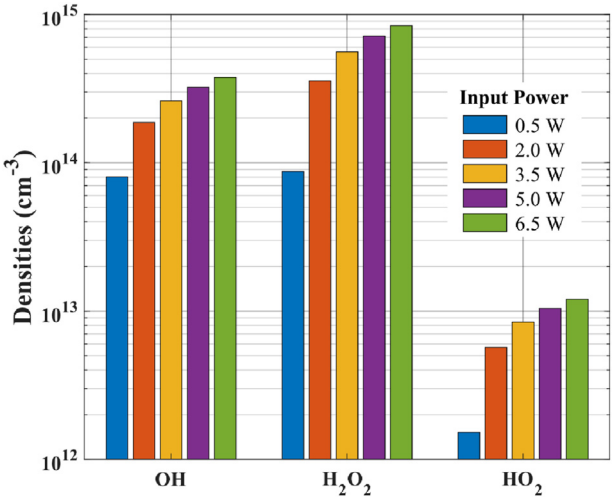

Fig. 9. Important species densities, in cm^{-3}, with different input power levels, in W.

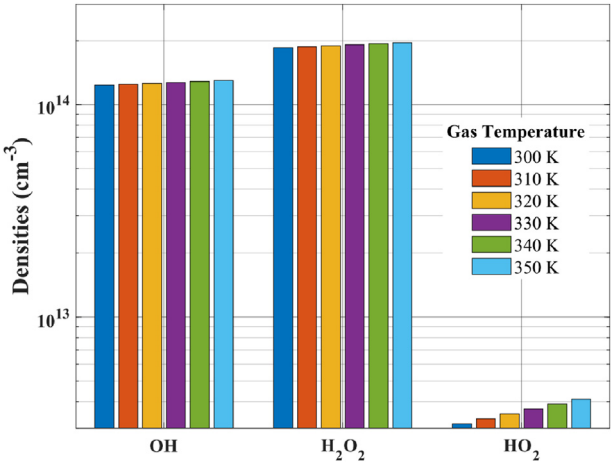

Fig. 10. Important species densities, in cm^{-3}, with different gas temperature, in K.

density but with a more steep increase in the first stage. The behavior of species density with input power seems to reach saturation values at input power that was not reached in the present simulation. Simulation results demonstrates that the increase in input power over 2 W has small benefit with respect to increasing the gas discharge yield.

3.5. Important species density variation with gas temperature

Low temperature treatment is one of the most important features of atmospheric pressure glow discharge specially in the case of treating heat sensitive materials. So that the effect of gas temperature on the plasma reactivity has to be investigated. The effect of gas temperature variation has been investigated in the preset section by changing it in the range from 300 to 350 K. Figure 10 shows the relation between OH, H_2O_2, and HO_2 densities and the working gas temperature. The Densities of both OH and H_2O_2 show a slight increase with gas temperature but on the other hand, the density of HO_2 shows a significant growth. Simulation results establish that gas temperature generally has a negligible effect on the yield of OH and H_2O_2 and a small one on HO_2, so that high efficient system cooling is more preferred for treating heat-sensitive materials, with no effect on the discharge yield.

3.6. Important species density variation with gap distance

Gap distance is one of the parameters that control the amount of gas that can be treated in a gas discharge. Accordingly studying the effect of gap distance on the important reactive species yield has to be investigated to get a picture about the treatment rate Fig. 11.

Increasing the gap distance from 0.5 to 1.7 mm generally decreases the density of important reactive species. In the case of OH and H_2O_2 densities, increasing the gap distance moderately decreases the density but on the other hand, it decreases the density of HO_2 more steeply. The former discussion demonstrates that increasing the gap distance has a small decreasing effect on the system yield, so a tradeoff between the system yield and the treated amount of gas would be preferable depending on the targeted application. Rising the treatment rate can be achieved by using many devices in parallel.

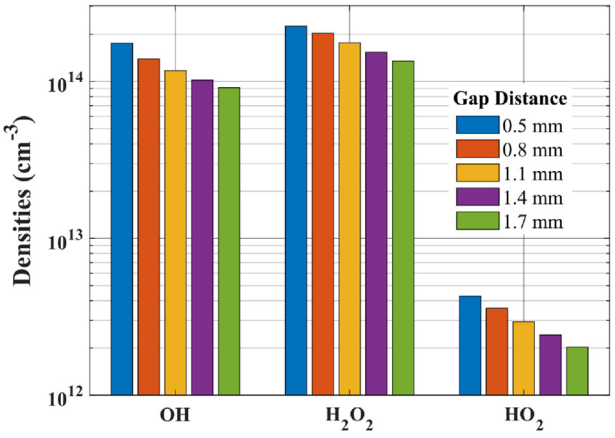

Fig. 11. Important species densities, in cm^{-3}, with different gap distances, in mm.

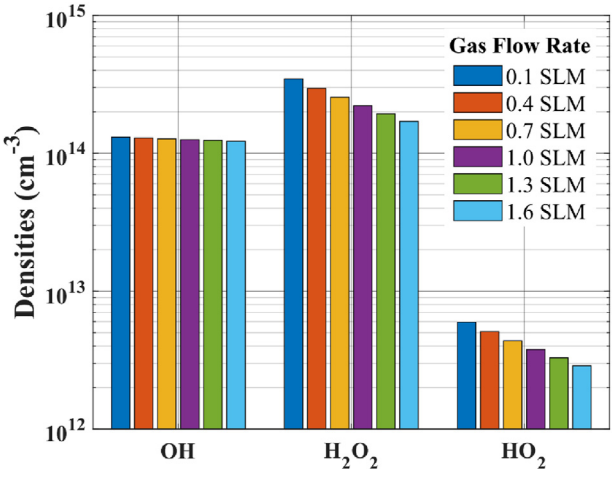

Fig. 12. Important species densities, in cm^{-3}, with different gas flow rates, in SLM.

3.7. Important species density variation with gas flow rate

Gas flow rate is one of the most important features of atmospheric pressure plasma jets, as it controls the process of delivering important reactive species to the treated targets, also controls the residence time of plasma species under the effect of the applied field. Accordingly, the effect of change in gas flow rate on the important species densities will be investigated in the present section.

Rising the gas flow rate from 0.1 to 1.6 SLM has been applied to investigate its effect on the densities of important reactive species. The density of OH radical shows no response to the change in flow rate in the considered range of variation. However, the densities of both H_2O_2 and HO_2 has a decreasing behavior with increasing the gas flow rate. It can be seen from Fig. 12 that HO_2 has a more quenching effect with the increase in gas flow rate than that for H_2O_2 density. The different behavior between OH and the other two species could be explained according to the high reactivity of OH species leading to steady state densities in a short time and so its density did not change with the flow rate (residence time). On the other hand, increasing the flow rate decreases the residence time of the treated gas under the effect of the applied field and so reduces the yield of H_2O_2 and HO_2. As in the case of gap distance change, a trade between the distribution of species in the system yield and the treated amount of gas would be preferable depending on the targeted application.

4. Conclusion

Water as a gas additive to working gas in discharge systems is one of the most promising precursors. In the present paper we have proposed a chemical kinetic global model to simulate gas discharge systems in the existence of different humidity levels. In order to ensure the results of the present model a comparison between the proposed model and both simulation [47] and experimental data [34] has been applied. According to comparison between the proposed model and the experimental measurements the reliability of the present model has been established.

As we ensures the reliability of our model we start to compare between our model output for reactive species and the simulation results of the simulation model in Ref. [47]. Short-lived species has generally greater density in the output of the proposed model than that obtained according to the simulation with the model in Ref. [47], except for He* and OH (A). Negative ions densities obtained from the proposed model are generally less than what we got according to the simulation model in Ref. [47], except for the case of O_2^-. Positive ions densities obtained from the proposed model are generally greater than that obtained from the simulation model in Ref. [47], except for the case of H_2O^+ and OH^+. Positive ion water cluster densities obtained from the proposed model generally are greater than that found in the model in Ref. [47], except for the case of $H_5O_2^+$.

After comparing the two models' results and for more assurance about the proposed model results relevance and applicability of the study's findings to real-world scenarios. We applied a comparison between the model's simulation results and experimental data in Ref. [56], for the effect of varying the input power to the system on the density of O_3 species, in the next section. It was demonstrated that the simulation model stands for the experimental data in both qualitative and quantitative manner.

As we demonstrate the applicability of the model results to real-world scenarios, we start to investigate the effect of different input parameters on the densities of some important reactive species (OH, H_2O_2, and HO_2). Input power to the model was varied in the range from 0.5 to 6.5 W. The density of OH radical rises sharply as the input power changes from 0.5 to 2 W but as the input power increases over the OH density slightly grows. The densities of both H_2O_2 and HO_2 shows the same behavior as the OH density but with more steep increase in the first stage. Gas temperature variation in the range from 300 to 350 K slightly increases the densities of both OH and H_2O_2 but on the other hand, the density of HO_2 shows a significant growth. Increasing the gap distance from 0.5 to 1.7 mm generally decreases the densities of OH and H_2O_2 moderately but on the other hand it decreases the density of HO_2 in a more

declining manner. Rising the gas flow rate from 0.1 to 1.6 SLM does not affect the density of OH radical in the considered range of variation. However, the densities of both H_2O_2 and HO_2 show a diminishing behavior with raising the gas flow rate.

Finally, we can come out with some conclusions from the present work which will be reported in the attending paragraph. The proposed simulation model can be used in simulating chemical kinetics in gas discharge plasma with satisfying results in both qualitative and quantitative levels. Rising the input power increases the yield of the system but rising it over 2W has no benefit. Keeping the gas temperature at 300 K has a small effect on the system yield. Using small gap distances can increase the yield of the system so to rise the treatment rate we can use many devices in parallel. Gas flow rate can be chosen according to the proposed application.

Author contribution

Osama Ahmed Shabaek developed the theory, performed the computations, implements the model into MATLAB code and wrote the manuscript in the first form. Dr. Farouk Fahmi Elakshar and Dr. Osama Mohamed Yassin conceived of the presented idea, verified the analytical methods and supervised the work. All authors discussed the results and contributed to the final manuscript.

Conflicts of interest

There are no conflicts of interest.

References

[1] Šimek M, Černák M, Kylián O, Foest R, Hegemann D, Martini R. White paper on the future of plasma science for optics and glass. Plasma Process Polym 2019;16:1700238.
[2] Bekeschus S, Favia P, Robert E, von Woedtke T. White paper on plasma for medicine and hygiene: future in plasma health sciences. Plasma Process Polym 2019;16:1800033.
[3] Stefan MI. Advanced Oxidation Processes for Water Treatment: Fundamentals and Applications. IWA publishing; 2017.
[4] Margot J, Kienle C, Magnet A, Weil M, Rossi L, de Alencastro LF, et al. Treatment of micropollutants in municipal wastewater: ozone or powdered activated carbon? Sci Total Environ 2013;461−462:480−98.
[5] Hughes WB, Younker CL. Organic Compounds Assessed in Chattahoochee River Water Used for Public Supply Near Atlanta, Georgia, 2004-05. US Department of the Interior, US Geological Survey; 2011.
[6] Locke BR, Shih KY. Review of the methods to form hydrogen peroxide in electrical discharge plasma with liquid water. Plasma Sources Sci Technol 2011;20:34006.
[7] Oller I, Malato S, Sánchez-Pérez JA. Combination of Advanced Oxidation Processes and biological treatments for wastewater decontamination-A review. Sci Total Environ 2011;409:4141−66.
[8] Bruggeman P, Leys C. Non-thermal plasmas in and in contact with liquids. J Phys D Appl Phys 2009;42:53001.
[9] Barbosa VL, Tandlich R, Burgess JE. Bioremediation of trace organic compounds found in precious metals refineries' wastewaters: a review of potential options. Chemosphere 2007;68:1195−203.
[10] Ganguli A, Prakash GV, Kar S, Sahu D, Others. A 2D steady state analytical model for atmospheric pressure RF plasma jet. Phys Scripta 2023;98:105011.
[11] Ning W, Shang H, Ji Y, Li R, Zhao L, Huang X, Jia S. Global model of plasma-activated water over long time scale: pulsed discharge and afterglow. High Volt 2023;8:326−39.
[12] Mahreen GV, Prakash S, Kar D, Sahu A, Ganguli. Influence of pulse modulation frequency on helium RF atmospheric pressure plasma jet characteristics. Contrib Plasma Phys 2022;62:e202200007.
[13] Tijani JO, Fatoba OO, Madzivire G, Petrik LF. A review of combined advanced oxidation technologies for the removal of organic pollutants from water. Water Air Soil Pollut 2014; 225:1−30.
[14] (Ken) Ostrikov K, Zhou R, Zhou R, Wang P, Xian Y, Mai-Prochnow A, et al. Plasma-activated water: generation, origin of reactive species and biological applications. J Phys D Appl Phys 2020;53:303001.
[15] Brandenburg R, Bogaerts A, Bongers W, Fridman A, Fridman G, Locke BR, et al. White paper on the future of plasma science in environment, for gas conversion and agriculture. Plasma Process Polym 2019;16:1700238.
[16] Foster JE. Plasma-based water purification: challenges and prospects for the future. Phys Plasmas 2017;24.
[17] Stratton GR, Dai F, Bellona CL, Holsen TM, Dickenson ERV, Mededovic Thagard S. Plasma-based water treatment: efficient transformation of perfluoroalkyl substances in prepared solutions and contaminated groundwater. Environ Sci Technol 2017;51:1643−8.
[18] TP R, Kar S. Effect of an additional floating electrode on radio frequency cross-field atmospheric pressure plasma jet. Sci Rep 2023;13:10665.
[19] Bruggeman P, Iza F, Lauwers D, Gonzalvo YA. Mass spectrometry study of positive and negative ions in a capacitively coupled atmospheric pressure RF excited glow discharge in He−water mixtures. J Phys D Appl Phys 2010;43:012003.
[20] Knake N, Niemi K, Reuter S, der Gathen V, Winter J. Absolute atomic oxygen density profiles in the discharge core of a microscale atmospheric pressure plasma jet. Appl Phys Lett 2008;93:13.
[21] Chung H, Ku B, Gregory J. Development of an advanced water treatment system for wastewater reuse. Environ Technol 2008;29:931−9.
[22] Gordillo-Vázquez FJ. Air plasma kinetics under the influence of sprites. J Phys D Appl Phys 2008;41:234016.
[23] Knake N, Reuter S, Niemi K, Schulz-Von Der Gathen V, Winter J. Absolute atomic oxygen density distributions in the effluent of a microscale atmospheric pressure plasma jet. J Phys D Appl Phys 2008;41:19.
[24] Lieberman MA, Lichtenberg AJ. Principles of plasma discharges and materials processing. In: Princ Plasma Discharges Mater Process Second Ed. second ed.30; 2005. p. 1−757.
[25] Savin YV, Goryachev LV, Adamenkov YA, Rakhimova TV, Mankelevich YA, Popov NA, et al. Singlet oxygen production and quenching mechanisms in travelling microwave discharges. J Phys D Appl Phys 2004;37:3121−8.
[26] Czerwiec T, Gavillet J, Belmonte T, Michel H, Ricard A. Determination of N and O atom density in Ar-N2-H2and Ar-O2-H2 flowing microwave post discharges. J Phys III 1996;6: 1205−12.
[27] Axforof SDT, Hayhurst AN. Mass spectrometric sampling of negative ions from flames of hydrogen and oxygen: the kinetics of electron attachment and detachment in hot mixtures of H2O, O2, OH and HO2. Proc RSoc A Math Phys Eng Sci 1948 1996;452:1007−33.
[28] Arrowsmith CD, Dyson A, Gudmundsson JT, Bingham R, Gregori G. Inductively-coupled plasma discharge for use in high-energy-density science experiments. J Instrum 2023;18: P04008.

[29] Scott CD, Farhat S, Gicquel A, Hassouni K, Lefebvre M. Determining electron temperature and density in a hydrogen microwave plasma. AIAA 24th Plasma Dyn Lasers Conf 1993 1993;10:426−35.
[30] Hadj-Ziane S, Held B, Pignole P, Peyrous R, Coster C. Ozone generation in an oxygen-fed wire-to-cylinder ozonizer at atmospheric pressure. J Phys D Appl Phys 1992;25:677−85.
[31] Bittner J, Kohse-Höinghaus K, Meier U, Just T. Quenching of two-photon-excited H (3s, 3d) and O (3p 3P2, 1, 0) atoms by rare gases and small molecules. Chem Phys Lett 1988;143: 571−6.
[32] Rowe BR, Vallée F, Queffelec JL, Gomet JC, Morlais M. The yield of oxygen and hydrogen atoms through dissociative recombination of H2O+ ions with electrons. J Chem Phys 1988;88:845−50.
[33] Invernizzi L, Muja C, Sainct FP, Guillot P. Investigation of RONS production and complex molecules degradation induced by an APPJ generated by two different sources. IEEE Trans Radiat Plasma Med Sci 2019;4:121−9.
[34] Benedikt J, Schröder D, Schneider S, Willems G, Pajdarová A, Vlček J, et al. Absolute OH and O radical densities in effluent of a He/H2O micro-scaled atmospheric pressure plasma jet. Plasma Sources Sci Technol 2016;25: 45013.
[35] Golda J, Held J, Redeker B, Konkowski M, Beijer P, Sobota A, et al. Concepts and characteristics of the COST reference microplasma jet. J Phys D Appl Phys 2016;49:84003.
[36] Turner MM. Uncertainty and sensitivity analysis in complex plasma chemistry models. Plasma Sources Sci Technol 2016; 25:15003.
[37] Turner MM. Uncertainty and error in complex plasma chemistry models. Plasma Sources Sci Technol 2015;24:35027.
[38] Reuter S, Tresp H, Wende K, Hammer MU, Winter J, Masur K, et al. From RONS to ROS: tailoring plasma jet treatment of skin cells. IEEE Trans Plasma Sci 2012;40(11 PART2):2986−93. 40.
[39] Hung PC, Chang SH, Chi KH, Chang MB. Degradation of gaseous dioxin-like compounds with dielectric barrier discharges. J Hazard Mater 2010;182:246−51.
[40] Ding K, Lieberman MA, Lichtenberg AJ. Hybrid model of neutral diffusion, sheaths, and the α to γ transition in an atmospheric pressure He/H2O bounded rf discharge. J Phys D Appl Phys 2014;47:305203.
[41] Murakami T, Niemi K, Gans T, O'Connell D, Graham WG. Interacting kinetics of neutral and ionic species in an atmospheric-pressure helium-oxygen plasma with humid air impurities. Plasma Sources Sci Technol 2013;22:45010.
[42] Liu DX, Iza F, Wang XH, Ma ZZ, Rong MZ, Kong MG. A theoretical insight into low-temperature atmospheric-pressure He+H2 plasmas. Plasma Sci Technol 2013;22:55016.
[43] Van Gaens W, Bogaerts A. Kinetic modelling for an atmospheric pressure argon plasma jet in humid air. J Phys D Appl Phys 2013;46:275201.
[44] Murakami T, Niemi K, Gans T, O'Connell D, Graham WG. Chemical kinetics and reactive species in atmospheric pressure helium-oxygen plasmas with humid-air impurities. Plasma Sources Sci Technol 2013;22:15003.
[45] Murakami T, Niemi K, Gans T, O'Connell D, Graham WG. Reactive species in atmospheric pressure helium-oxygen plasmas with humid air impurities. APS Annu Gaseous Electron Meet Abstr 2012:QR2−Q2001.
[46] Dunlea EJ, Talukdar RK, Ravishankara AR. Kinetic studies of the reactions of O2(b 1Σg+) with several atmospheric molecules. J Phys Chem A 2005;109:3912−20.
[47] Liu D-X, Bruggeman P, Iza F, Rong M-Z, Kong MG. Global model of low-temperature atmospheric-pressure He+H2O plasmas. Plasma Sources Sci Technol 2010;19:25018.
[48] Liu DX, Iza F, Wang XH, Kong MG, Rong MZ. He+ O2+H2O plasmas as a source of reactive oxygen species. Appl Phys Lett 2011;98:22.
[49] Liu D, Sun B, Iza F, Xu D, Wang X, Rong M, Kong MG. Main species and chemical pathways in cold atmospheric-pressure Ar + H2O plasmas. Plasma Sources Sci Technol 2017;26:45009.
[50] Naidis GV. Modelling of OH production in cold atmospheric-pressure He-H2O plasma jets. Plasma Sources Sci Technol 2013;22:35015.
[51] Brisset A, Gibson AR, Schröter S, Niemi K, Booth JP, Gans T, et al. Chemical kinetics and density measurements of OH in an atmospheric pressure He + O2+ H2O radiofrequency plasma. J Phys D Appl Phys 2021;54:285201.
[52] Sun J, Zhang T, Hong J, Zhou R, Masood H, Zhou R, et al. Insights into plasma-catalytic nitrogen fixation from catalyst microanalysis and chemical kinetics modelling. Chem Eng J 2023;469:143841.
[53] Zhou XF, Geng WQ, Ma XY, Ran CF, Liu K. Dynamics of NO, N2O, and ONOOH in atmospheric-pressure air dielectric barrier discharge: decoupling energy density and gas temperature effects varying with discharge voltage. J Phys D Appl Phys 2024;57:21.
[54] Mendez I, Gordillo-Vázquez FJ, Herrero VJ, Tanarro I. Atom and ion chemistry in low pressure hydrogen DC plasmas. J Phys Chem A 2006;110:6060−6.
[55] Stafford DS, Kushner MJ. O2(1Δ) production in He/O2 mixtures in flowing low pressure plasmas. J Appl Phys 2004; 96:2451−65.
[56] Wijaikhum A, Schröder D, Schröter S, Gibson AR, Niemi K, Friderich J, et al. Absolute ozone densities in a radio-frequency driven atmospheric pressure plasma using two-beam UV-LED absorption spectroscopy and numerical simulations. Plasma Sources Sci Technol 2017;26:115004.